Gamow-Teller transition strengths from ^{56}Fe extracted from the ^{56}Fe(t,^{3}He) reaction

M. Scott,[1,2,3] Y. Shimbara,[4,*] Sam M. Austin,[1,3] D. Bazin,[1] B. A. Brown,[1,2,3] J. M. Deaven,[1,2,3,†] Y. Fujita,[5,6] C. J. Guess,[7,‡] S. Gupta,[8] G. W. Hitt,[9] D. Koeppe,[1,2,3] R. Meharchand,[1,2,3,§] M. Nagashima,[4] G. Perdikakis,[3,10] A. Prinke,[1,2,3,‖] M. Sasano,[1,2,3,¶] C. Sullivan,[1,2,3] L. Valdez,[1,2,3,**] and R. G. T. Zegers[1,2,3,††]

[1]*National Superconducting Cyclotron Laboratory, Michigan State University, East Lansing, Michigan 48824, USA*
[2]*Department of Physics and Astronomy, Michigan State University, East Lansing, Michigan 48824, USA*
[3]*Joint Institute for Nuclear Astrophysics, Michigan State University, East Lansing, Michigan 48824, USA*
[4]*Graduate School of Science and Technology, Niigata University, Niigata 950-2181, Japan*
[5]*Department of Physics, Osaka University, Toyonaka, Osaka 560-0043, Japan*
[6]*Research Center for Nuclear Physics, Osaka University, Ibaraki, Osaka 567-0047, Japan*
[7]*Department of Physics and Applied Physics, University of Massachusetts Lowell, Lowell, Massachusetts 01854, USA*
[8]*Indian Institute of Technology, IIT Ropar, Punjab, 140001, India*
[9]*Department of Applied Mathematics and Sciences, Khalifa University of Science, Technology, and Research, P.O. Box 127788, Abu Dhabi, UAE*
[10]*Department of Physics, Central Michigan University, Mt. Pleasant, Michigan 48859, USA*

(Received 5 February 2014; revised manuscript received 26 May 2014; published 4 August 2014)

Background: Gamow-Teller (GT) transition strengths are key inputs for estimating weak reaction rates of importance for a wide variety of astrophysical applications. (n,p)-type charge-exchange reactions, such as the (t,^{3}He) reaction used in this work, are commonly used for extracting the GT strength distribution in the β^+ (electron-capture) direction. Such studies are important for testing theoretical models used to estimate weak rates for a large number of nuclei for simulations of astrophysical phenomena.
Purpose: The ^{56}Fe(t,^{3}He) reaction at 115 A MeV was measured in order to extract GT strengths for transitions to ^{56}Mn. The extracted strength distributions were compared with shell-model calculations in the pf-shell model space using the KB3G and GXPF1a interactions, and with calculations in the quasi-particle random-phase approximation (QRPA).
Method: Differential cross sections and excitation-energy spectra for the ^{56}Fe(t,^{3}He) reaction were determined by measuring the trajectories of ^{3}He ejectiles through the S800 magnetic spectrograph and deducing their momenta. Contributions corresponding to GT transitions were isolated by using a multipole decomposition analysis. A well-established proportionality between GT strength and differential cross section at zero-linear-momentum transfer was utilized to convert extracted cross sections to GT strengths.
Results and Conclusions: GT transition strengths from ^{56}Fe to ^{56}Mn were extracted up to an excitation energy of 10 MeV. Shell-model calculations with the GXPF1a interaction reproduced the observed GT strength distribution slightly better than calculations with the KB3G interaction. The calculated strength distribution in the QRPA did not reproduce the observed strength distribution. The new experimental data have an improved precision at low excitation energies compared to previous results obtained from an ^{56}Fe(n,p) experiment. Electron-capture rates based on the experimental and theoretical Gamow-Teller strengths were compared and deviations were included in an assessment of the validity of electron-capture rates based on theoretical models for nuclei in the pf shell.

DOI: 10.1103/PhysRevC.90.025801 PACS number(s): 21.60.Cs, 23.40.−s, 25.40.Kv, 26.30.Jk

I. INTRODUCTION

Reactions mediated by the weak nuclear force play an important role in a wide variety of astrophysical phenomena (for an overview, see Ref. [1] and references therein). Electron captures are especially important in high-temperature and high-density sites, such as core-collapse (type II) [1–5] and thermonuclear (type Ia) supernovae [6,7], as well as in the crusts of neutron stars [8,9]. An enormous effort is devoted to modeling the stellar evolution, both quiescent and explosive, of these astrophysical sites, as they are major contributors to nucleosynthetic processes. Use of accurate weak reaction rates in simulations is necessary for obtaining realistic results, but it is not possible to determine all relevant reaction rates experimentally. Many nuclei, stable and unstable, are involved in the stellar evolution. In addition, in high-temperature stellar environments, transitions from thermally excited levels must

*Present address: Cyclotron and Radioisotope Center, Tohoku University, Aoba-ku, Sendai, Miyagi 980-8578, Japan.
†Present address: Department of Nuclear Engineering and Health Physics, Idaho State University, Idaho 83208, USA.
‡Present address: Department of Physics and Astronomy, Rowan University, Glassboro, New Jersey 08028, USA.
§Present address: Los Alamos National Laboratory, Los Alamos, New Mexico 87545, USA.
‖Present address: Pacific Northwest National Laboratory, 902 Battelle Boulevard, Richland, Washington 99352, USA.
¶Present address: RIKEN Nishina Center, 2-1 Hirosawa, Wako, Saitama 351-0198, Japan.
**Present address: Orange High School, 400 Lincoln Ave, City of Orange, New Jersey 07050, USA.
††zegers@nscl.msu.edu

be taken into account. To make progress, theoretical models are used for estimating weak reaction rates, and these models are benchmarked by targeted experimental efforts.

The most important inputs for estimating weak reaction rates as a function of electron density and temperature are Gamow-Teller (GT) strength distributions, which are associated with nuclear excitations in which spin ($\Delta S = 1$) and isospin ($\Delta T = 1$) are transferred, but no angular momentum is transferred ($\Delta L = 0$). Gamow-Teller transition strengths in the β^+ direction yield electron-capture (EC) rates. Most theoretical and experimental efforts aimed at estimating and testing electron-capture rates have focused on nuclei in the pf shell that play important roles in all of the aforementioned astrophysical phenomena [1–9]. Early rate estimates, the so-called Fuller, Fowler, and Newman (FFN) rates [10–13], were based on an independent-particle model. With the realization that better accuracies are required, more sophisticated nuclear models were used, in particular shell models with effective interactions and quasi-particle random phase approximation (QRPA) models [14–18].

Theoretical GT strengths can be tested by comparing to data from β-decay experiments, but only transitions associated with a positive-Q-value window are accessible in such experiments. Charge-exchange reactions at intermediate energies ($E_{\text{beam}} \gtrsim 100$ A MeV), from which GT strength distributions up to high excitation energies can be extracted, have therefore become the preferred tool for testing the theoretical models [19,20]. Recently, the results from (n,p), $(d,{}^2\text{He})$, and $(t,{}^3\text{He})$ reactions on nuclei in the pf shell were summarized [21] and systematically compared with shell-model calculations using the KB3G [22] and GXPF1a [23] effective interactions in the pf-model space, and with calculations in QRPA based on the formalism of Ref. [14]. That summary showed that both sets of shell-model calculations do rather well in reproducing experimentally extracted GT strength distributions, and derived electron-capture rates had averaged absolute deviations of less than 40% over wide temperature and density ranges of relevance for astrophysical simulations. A recent experiment focused on extracting the GT transition strength from ^{56}Ni [24,25] laid bare some of the key differences between the two above-mentioned shell-model calculations and indicated that the GXPF1a interaction performs slightly better. The QRPA calculations did not reproduce the experimental GT strength distributions as well and the derived electron-capture rates had much larger errors. On the other hand, QRPA calculations can be used for nuclei beyond the pf shell, where shell-model calculations still pose a significant challenge.

This work focuses on the GT strength in the β^+ direction for ^{56}Fe. The GT strength distribution from ^{56}Fe, populating states in ^{56}Mn, had previously been extracted in (n,p) experiments [26,27]. ^{56}Fe was included in the review of Ref. [21], but the relatively poor experimental resolution made it difficult to include ^{56}Fe in the quantitative comparisons between data and theory. In the present work, the ^{56}Fe$(t,{}^3\text{He})$ reaction at 115 A MeV incident triton energy was used to extract the GT transition strength from ^{56}Fe to ^{56}Mn with improved resolution, and the overall quantitative comparison between data and theory for nuclei in the pf shell was updated to include this case.

II. EXPERIMENT

A primary beam of $^{16}O^{8+}$ ions at 150 A MeV produced at the National Superconducting Cyclotron Laboratory (NSCL) Coupled Cyclotron Facility (CCF) [28] was impinged upon a 3526 mg/cm^2 thick beryllium target to produce a 115-A MeV secondary triton beam. An isotopic purity of better than 99% was obtained in the A1900 fragment separator [29], by placing a 195 mg/cm^2 thick aluminum wedge in the intermediate image to remove contaminants [30]. Slits were placed at the intermediate image of the A1900 to restrict the momentum acceptance to $\frac{dp}{p} = \pm 0.25\%$. A triton beam intensity of, on average, 7×10^6 particles/s was achieved. Details of the triton beam production at NSCL can be found in Refs. [30,31].

A 9.62 mg/cm^2 thick ^{56}Fe foil, with an isotopic purity of 99.93%, was placed at the pivot point of the S800 spectrograph [32], set for a central scattering angle of 0°. To optimize the energy resolution, the analysis beam line leading to the target was operated in dispersion-matched mode [33]. The $^3\text{He}^{2+}$ ejectiles from the $(t,{}^3\text{He})$ reactions were momentum-analyzed in the S800 focal plane [34], using the same setup as in Refs. [30,35]. For an unambiguous identification of the ^{3}He particles, the energy loss of reaction products produced at the target was measured in a plastic scintillator placed in the S800 focal plane and plotted against the time of flight (TOF) to the focal plane, relative to the CCF radio frequency (RF) signal. Using the code COSY INFINITY [36], a fifth-order inverse ion-optical transfer matrix was used to reconstruct the momenta and scattering angles of the ^{3}He particles produced at the target, based on positions and angles measured in tracking detectors in the S800 focal plane. The excitation-energy resolution obtained was 480 keV [full width at half maximum (FWHM)], which is significantly better than in the available (n,p) data. Events with scattering angles less than 6° in the center of mass were included in the analysis. The scattering angle resolution was 10 mrad (FWHM).

Absolute differential cross sections are needed to obtain absolute GT strengths. Cross sections were determined relative to those of the $^{12}\text{C}(t,{}^3\text{He})^{12}\text{B}(1^+,\text{g.s.})$ reaction for which accurate absolute cross sections were measured previously [37]. For that purpose, data were taken on the same 10 mg/cm^2 CH_2 foil used for measuring the absolute $^{12}\text{C}(t,{}^3\text{He})^{12}\text{B}(1^+,\text{g.s.})$ cross section. These data were used to correlate the triton beam intensity with the current of the ^{16}O primary beam measured in a nonintercepting probe, which was placed just after the cyclotrons. By carefully monitoring the nonintercepting probe, and correcting for relative changes in beam intensity, as well as for data-acquisition dead times and focal-plane detector efficiencies, the cross sections for the ^{56}Fe$(t,{}^3\text{He})$ reaction were determined.

III. DATA ANALYSIS

Extraction of GT transition strengths requires the isolation of transitions from the 0^+ ^{56}Fe ground state to 1^+ states in ^{56}Mn associated with $\Delta S = 1$ and $\Delta L = 0$. A multipole decomposition analysis (MDA) was performed to separate the yield associated with $\Delta L = 0$ transitions from transitions associated with $\Delta L > 0$, as described in Sec. III A. This

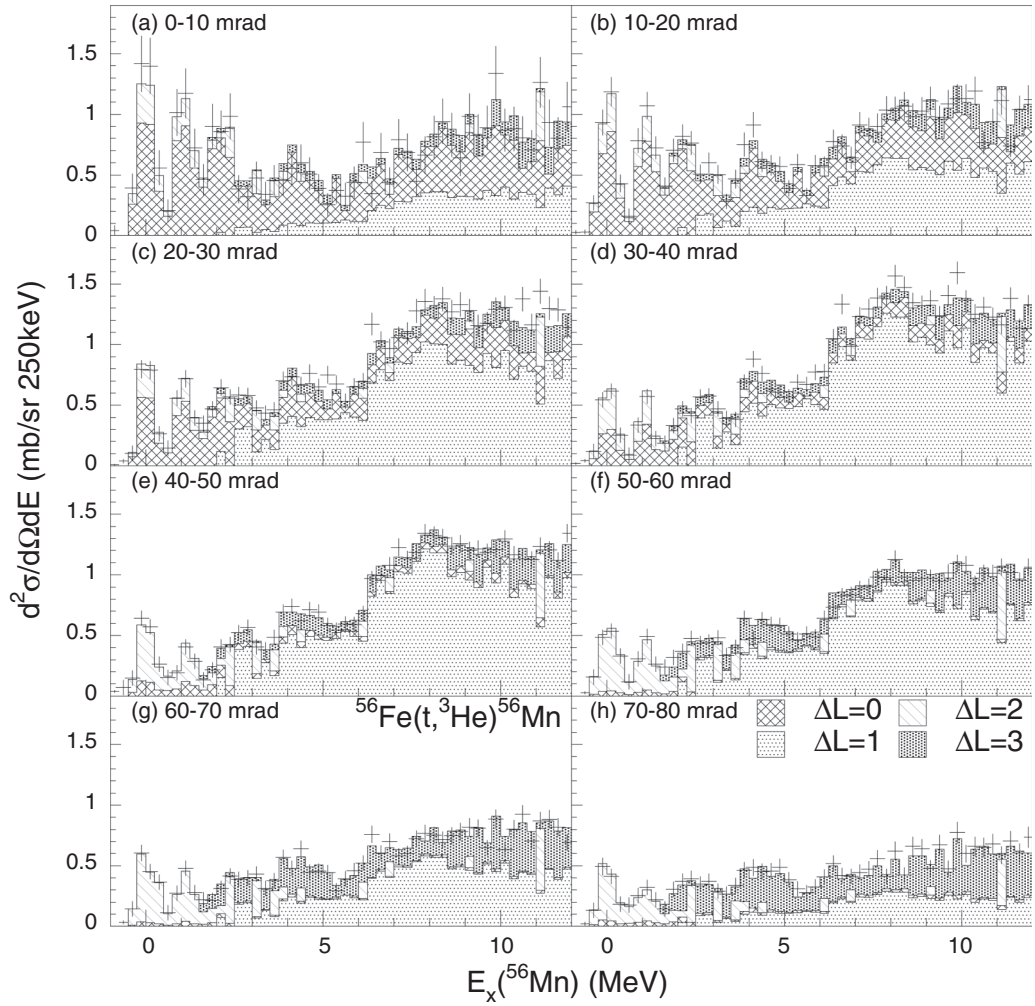

FIG. 1. Differential cross section for the ^{56}Fe(t,^{3}He) reaction, plotted as a function of excitation energy in ^{56}Mn. The spectrum is plotted for angular bins observed in the laboratory frame (in millirads). The observed spectrum is shown as the data points, with the hatched regions containing the results of the MDA.

procedure also removed $\Delta S = 1, \Delta L = 2$ contributions to the cross section for transitions from $J^\pi = 0^+$ to 1^+ final states, but it cannot account for interference between $\Delta L = 0$ and $\Delta L = 2$ amplitudes. Such interference effects, which increase the systematic uncertainty of extracted Gamow-Teller strengths for weak transitions, have been studied in detail for the (^{3}He,t) and (t,^{3}He) reactions [35,38–41].

At $E_x \lesssim 10$ MeV all $\Delta L = 0$ strength can be associated with GT transitions, as the $\Delta S = 0, \Delta L = 0$ yield is negligible. At higher excitation energies, contributions from the excitation of the isovector (spin) giant monopole resonances ($\Delta L = 0$, $\Delta S = 0$ or 1, $2\hbar\omega$ excitations) can contaminate the Gamow-Teller response [20].

For $E_{\rm beam} \gtrsim 100$ A MeV, the $\Delta L = 0$ differential cross section in the limit of vanishing momentum transfer ($q = 0$) is proportional to B(GT) [42]:

$$\left(\frac{d\sigma}{d\Omega}\right)_{q\to 0} = \hat{\sigma}_{\rm GT} B({\rm GT}), \qquad (1)$$

where $\hat{\sigma}_{\rm GT}$ is the so-called unit cross section, determined from the empirical mass-dependent relationship of Refs. [37,40]. A detailed description of the extraction of strength can be found in Sec. III B.

A. Multipole decomposition analysis

Figure 1 shows the double-differential cross sections as a function of excitation energy in ^{56}Mn, for scattering-angle bins of 10 mrad in the laboratory frame, up to 80 mrad. The excitation-energy bin width is 250 keV. Transitions to two known 1^+ states at 0.11 and 1.17 MeV [43] can clearly be distinguished, and both are strongly populated. Since the location of these states is well known, the MDA was performed for each of these peaks separately and the associated GT strength placed at the corresponding excitation energies. At higher excitation energies, the MDA was performed for each 250-keV-wide bin.

Figure 2 is an example of the MDA for the peak at 1.17 MeV. The experimental differential cross section was fitted to a linear combination of angular distributions associated with different angular-momentum transfers. These angular distributions were generated in the distorted-wave Born

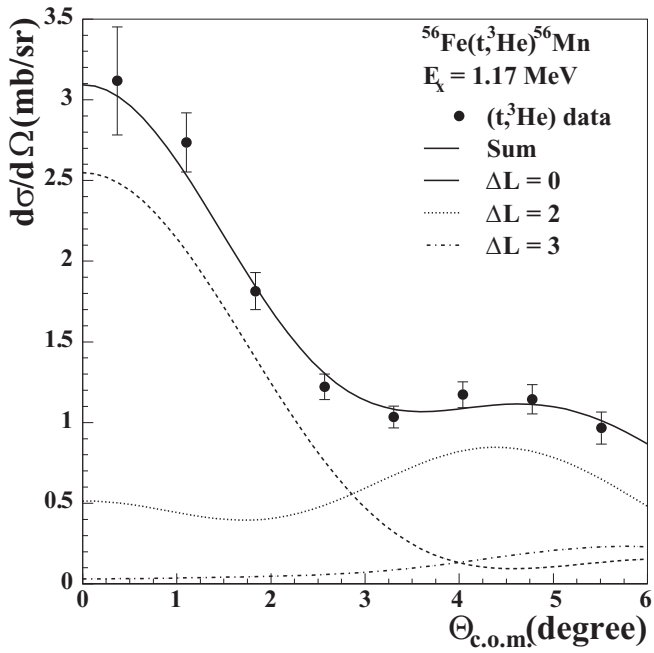

FIG. 2. Differential cross section for the peak observed at 1.17 MeV in the ^{56}Mn spectrum, with the results from the MDA superimposed. The cross section is dominated by a $\Delta L = 0$ component associated with the excitation of a known 1^+ state. The error bars only represent the statistical uncertainty associated with the number of events measured in each angular bin.

approximation (DWBA) formalism using the code package FOLD [44]. As inputs to the calculation, one-body transition densities (OBTDs) associated with different angular-momentum transfers were obtained in the normal-modes formalism using the code NORMOD [45]. Following previous analyses [37], single-particle binding energies for ^{56}Fe and ^{56}Mn, obtained from NUSHELLX@MSU [46] using the SK20 interaction [47], were used in the calculation of radial wave functions in a Woods-Saxon potential. For the t and ^{3}He particles, radial densities obtained from variational Monte Carlo calculations [48] were used and all protons and neutrons were assumed to be in the $1s_{1/2}$ orbit. The effective nucleon-nucleon interaction at 140 MeV from Love and Franey [49,50] was double-folded over the transition densities in the t-^{3}He and ^{56}Fe-^{56}Mn systems to produce form factors which served as inputs for the DWBA calculation. Optical-model parameters obtained for the exit channel were taken from ^{3}He elastic-scattering data on ^{58}Ni [51]. For the entrance channel, He well depths from Ref. [51] were scaled by a factor 0.85, following the procedure in Ref. [52].

At the beam energy of 115 A MeV, and at forward scattering angles, the contributions from excitations with $\Delta L > 3$ are small and have angular distributions not easily distinguishable from $\Delta L = 2$ or 3 transitions in the angular range under consideration. Hence, in the MDA, only contributions to the spectrum for $\Delta L = 0$, 1, 2, and 3 were considered in the fits. Figure 2 shows an example for the MDA for the peak at 1.17 MeV, which is predominantly associated with $\Delta L = 0$ but has a significant $\Delta L = 2$ component, as can be expected for a $0^+ \rightarrow 1^+$ transition (see, e.g., Ref. [37]). No statistically significant dipole ($\Delta L = 1$) contribution was observed for this particular fit, and the systematic uncertainties were small. A similar result was found for the excitation at 0.11 MeV and the broader peaks observed at 2 and 4 MeV also contained significant $\Delta L = 0$ contributions. At higher excitation energies, strong dipole contributions were found. When the dipole excitations become strong, the extraction of small GT contributions to the spectrum is complicated by the fact that the dipole transitions associated with $\Delta J = 0$, 1, and 2 have slightly different angular distributions at forward scattering angles. In combination with the limited statistical accuracy of the data, this resulted in a sizable systematic uncertainty (estimated by performing the MDA using the angular distribution for each for the dipole excitations separately, and comparing the results) for the extracted $\Delta L = 0$ component. In Fig. 1, the contributions from transitions with different angular-momentum transfers to the differential cross section spectra are indicated. In comparison to the angular distributions for $\Delta L = 0$ and 1 transitions, the differences between the angular distributions for $\Delta L = 2$ and 3 transitions are rather small at forward scattering angles. In addition, the extracted contributions for $\Delta L = 2$ and 3 transitions also contain contributions from transitions with $\Delta L > 3$. Consequently, contributions from $\Delta L = 2$ and 3 transitions can be misidentified (see the bin at $E_x = 11.25$ MeV in Fig. 1). One should thus refrain from using the extracted cross sections for $\Delta L > 1$ for making detailed interpretations.

B. Extraction of strength

After the differential cross sections for the $\Delta L = 0$ GT transitions were isolated, the corresponding transition strengths were extracted using Eq. (1). The proportionality in Eq. (1) is defined for the differential cross section at zero-linear-momentum transfer ($q = 0$), which occurs at $Q = 0$ and $\theta = 0^\circ$. Since $Q_{\text{g.s.}} = 3.677$ MeV, the extracted differential cross sections were extrapolated to $Q = 0$ on the basis of the DWBA calculations using the relation [37]

$$\left(\frac{d\sigma}{d\Omega}\right)_{q\rightarrow 0} = \left[\frac{\frac{d\sigma}{d\Omega}(Q=0,0^\circ)}{\frac{d\sigma}{d\Omega}(Q,0^\circ)}\right]_{\text{DWBA}} \left[\frac{d\sigma}{d\Omega}(Q,0^\circ)\right]_{\text{exp}}, \quad (2)$$

where the "DWBA" and "exp" subscripts denote the calculated and measured cross sections, respectively. To establish the ratio used in Eq. (2) as a smooth function of Q, the ratio was generated for 100 reaction Q values in the excitation energy range of interest.

The unit cross section $\hat{\sigma}_{\text{GT}}$ was calculated by using the empirical mass-dependent relationship [37,38]

$$\hat{\sigma}_{\text{GT}} = 109\, A^{-0.65}\ (\text{mb/sr}). \quad (3)$$

By using Eqs. (1), (2), and (3), B(GT) was extracted for the two low-lying states and each 250-keV-wide bin above 1.5 MeV. The results are presented in Fig. 3(a). The errors shown are from statistical and systematic uncertainties combined. At higher E_x ($E_x > 4$ MeV), where the dipole contributions are strong, the uncertainty in the extracted B(GT) is large.

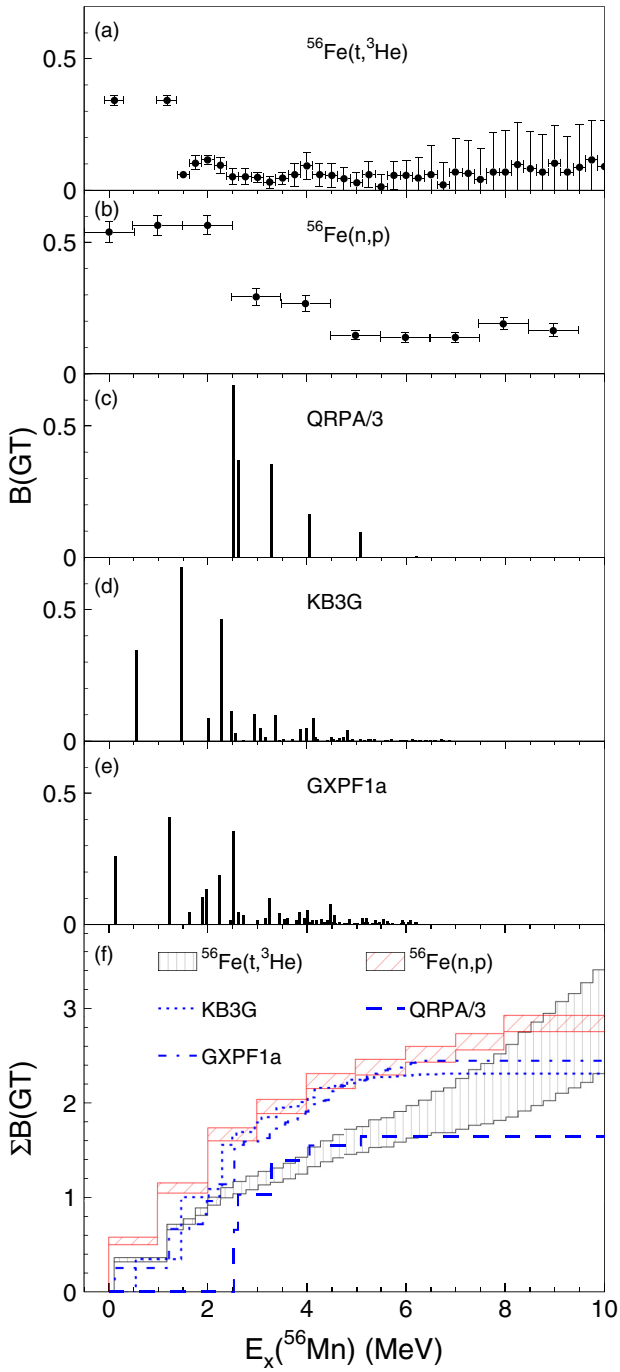

FIG. 3. (Color online) GT strength distributions from ^{56}Fe to ^{56}Mn (a) extracted from the ^{56}Fe$(t,^3$He) data (with horizontal bars indicating the 250-keV-wide energy bins, except for the peaks at 0.1 and 1.17 MeV, for which they indicate the accuracy with which the peak locations could be identified in the current data), (b) extracted from the ^{56}Fe(n,p) data (in 1-MeV bins, as indicated by the horizontal bars), (c) from calculations in the QRPA (divided by 3), (d) from shell-model calculations using the KB3G interaction, and (e) from shell-model calculations using the GXPF1a interaction. In (f), running sums of the GT strengths as a function of excitation energies are plotted. The hatched regions of the data represent the statistical and systematic uncertainties in the $(t,^3$He) data and the statistical uncertainty in the (n,p) data.

Figure 3(b) shows the extracted GT strength from the ^{56}Fe(n,p) reaction of Ref. [26], which had an excitation-energy resolution of 1.3 MeV (where the strength was extracted in 1-MeV-wide bins). The two low-lying, strongly excited 1^+ states could not be separated in these data. A second ^{56}Fe(n,p) experiment performed at 100 A MeV [27] had an excitation-energy resolution of 2.8 MeV and was not used for comparison in this analysis. Data from the ^{56}Fe$(d,^2$He) reaction are available [53] with high resolution (110 keV), but GT strengths were not reported. The main features of the ^{56}Fe$(d,^2$He) spectrum appear qualitatively compatible with the present results.

Figures 3(c)–3(e) show the results of the theoretical calculations in the QRPA and in the shell models using KB3G and GXPF1a interactions, respectively. A quenching factor of $(0.74)^2$ [54] was applied to the shell-model calculations, which were performed using the code NUSHELLX@MSU [46]. The QRPA calculations were based on the framework of Ref. [14] and use ground-state deformation parameters and masses from the finite-range droplet model of Ref. [55]. Following Ref. [14], a quenching factor was not applied to the calculated GT strengths.

Both shell-model calculations reproduce the low-lying states, with the GXPF1a interaction reproducing most accurately the location and strength of the first two 1^+ states. The QRPA results overestimate the total strength by about 50%, and, in contrast to the experiment, have no strength below an excitation energy of 2 MeV.

In Fig. 3(f), the running sums of the GT strengths as a function of excitation energy in ^{56}Mn are compared. We note that, even though at higher excitation energies the extracted GT strengths in the present data are consistent with zero, in all bins a consistent trend of finite amounts of GT strengths is found, giving rise to a slowly increasing summed strength, with increasing error margins. We also note that the (n,p) data have a 10% systematic uncertainty [26] due to the MDA, which is not plotted in Fig. 3. Both the (n,p) and present data have an additional 10% uncertainty in the unit cross section, which is also not shown in Fig. 3 [37,40,42].

Both shell-model calculations predict more strength between 2 and 3 MeV than seen in the ^{56}Fe$(t,^3$He) data, and consequently they overestimate the summed experimental strength up to 8 MeV. In comparison to the ^{56}Fe(n,p) data, the summed theoretical strengths from the shell models match quite well. We note that the somewhat better performance of the GXPF1a interaction compared to the KB3G interaction confirms the findings for neighboring nuclei ^{56}Ni and ^{55}Co [24,25].

IV. ELECTRON-CAPTURE RATES

To quantify the differences observed between the experimental and theoretical GT strength in terms of EC rates of relevance for late stellar evolution, we compared calculated EC rates based on these strength distributions for a wide range of temperatures and stellar densities, similar to the study of Ref. [21]. The calculations were performed using the FFN formalism [10–13] and implemented in a code previously used in Refs. [8,56]. Here, we present the results of the

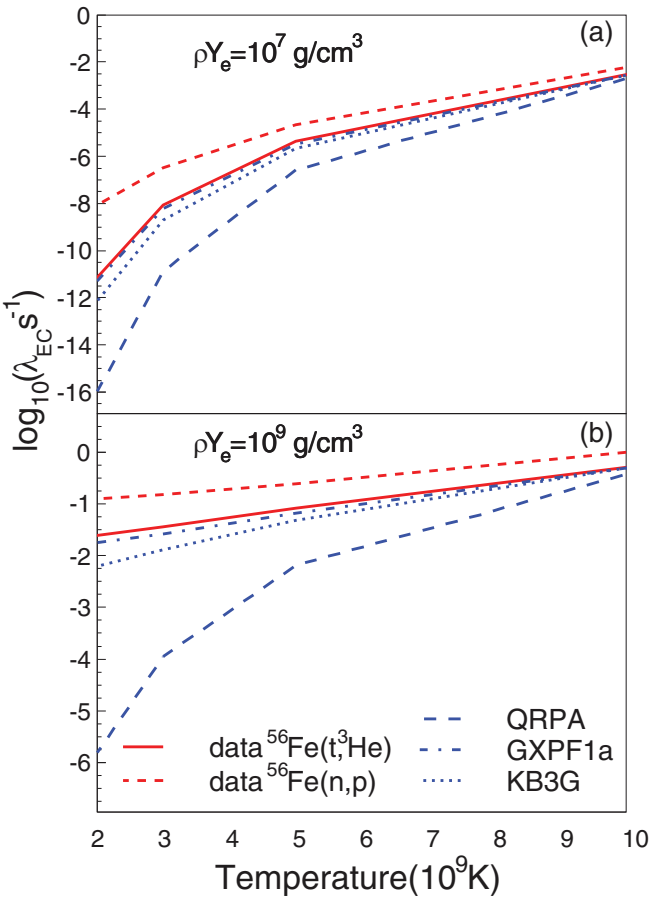

FIG. 4. (Color online) Electron-capture rates on ^{56}Fe derived from the experimental and theoretical GT strength distributions of Fig. 3 (a) at $\rho Y_e = 10^7$ g/cm^3 and (b) at $\rho Y_e = 10^9$ g/cm^3.

comparisons at two stellar densities. The lower of these densities ($\rho Y_e = 10^7$ g/cm^3, where ρ is the density and Y_e is the electron fraction, which is equal to the number of electrons per baryon) corresponds to conditions in a pre-core-collapse (type II) progenitor star [57], while the higher density of $\rho Y_e = 10^9$ g/cm^3 corresponds to conditions just prior to the collapse of the core [4,58] and to the high-density regions in which EC occurs in type Ia supernovae during the thermonuclear runaway [6,7].

The EC rates depend strongly on the exact excitation energies of transitions to low-lying final states, in particular at low stellar densities. Given that transitions to the two lowest-lying 1^+ states could not be separated in the ^{56}Fe(n,p) data and some strength was placed at artificially low excitation energies, the corresponding EC rates are systematically overestimated compared to the rates based on GT strengths extracted from the ^{56}Fe$(t,^3$He) data.

Because the excitation energies and strengths of the two low-lying 1^+ final states associated with strong GT strengths calculated in the shell model using the GXPF1a interaction match the ^{56}Fe$(t,^3$He) data well, the derived EC rates are close. Since the excitation energies of the first 1^+ states are too high in the shell-model calculation with the KB3G interaction, the derived EC rate based on this model is too low. The same holds, but to a much larger degree, for the EC rates based on the GT strength distribution calculated in the QRPA.

At the higher stellar densities, the EC rates become more sensitive to the GT strength distribution at higher excitation energies, and the differences between the EC rates based on the different data sets and theoretical calculations become smaller than at lower densities, as shown in Fig. 4. Nevertheless, the contribution from strong transitions to the two low-lying 1^+ states still dominates, and the main features observed at $\rho Y_e = 10^7$ g/cm^3 persist at $\rho Y_e = 10^9$ g/cm^3.

The present results from the ^{56}Fe$(t,^3$He) experiment were used to update the comparison between EC rates based on experimental and theoretical GT strength distributions presented in Ref. [21]. In Ref. [21], the following measures were used to evaluate the quality of the theoretically estimated rates in comparison to the rates based on experimental GT strength:

$$\overline{\Delta_{\rm EC}} = \frac{1}{N}\sum_{i=1}^{N}\frac{\lambda_i^{\rm th}-\lambda_i^{\rm exp}}{\lambda_i^{\rm exp}}, \tag{4}$$

$$\overline{|\Delta_{\rm EC}|} = \frac{1}{N}\sum_{i=1}^{N}\frac{|\lambda_i^{\rm th}-\lambda_i^{\rm exp}|}{\lambda_i^{\rm exp}}. \tag{5}$$

$\overline{\Delta_{\rm EC}}$ ($\overline{|\Delta_{\rm EC}|}$) is the average (absolute) deviation between the EC rates based on the charge-exchange data ($\lambda^{\rm exp}$) and the theory ($\lambda^{\rm th}$). The summations run over all nuclei for which high-resolution charge-exchange data are available.

TABLE I. Average deviations between EC rates calculated based on theoretical GT strength distributions and EC rates based on GT strengths extracted from charge-exchange experiments, relative to the experimental values [see Eqs. (4) and (5)], for two stellar density-temperature combinations. Considered were only EC rates on the ground states of eight nuclei (^{48}Ti, ^{51}V, ^{56}Fe, ^{58}Ni, ^{60}Ni, ^{62}Ni, ^{64}Ni, and ^{64}Zn) in the pf shell for which high-resolution data were available or the strength distribution at low excitation energies in the daughter nucleus were otherwise well defined. The left-hand side of the table refers to deviations at $\rho Y_e = 10^7$ g/cm^3 and a temperature of $T = 3\times10^9$ K (case I) and the right-hand-side of the table refers to deviations at $\rho Y_e = 10^9$ g/cm^3 and $T = 10\times10^9$ K (case II). For details refer to Ref. [21]. The current table is the same as that in Ref. [21], except that the new data for ^{56}Fe have been included, raising the number of available cases from seven to eight.

	I: $\rho Y_e = 10^7$ g/cm^3, $T = 3\times10^9$ K			II: $\rho Y_e = 10^9$ g/cm^3, $T = 10\times10^9$ K		
	GXPF1a	KB3G	QRPA	GXPF1a	KB3G	QRPA
$\overline{\Delta_{\rm EC}}$	−0.25	−0.40	26.	−0.05	0.01	0.54
$\overline{\lvert\Delta_{\rm EC}\rvert}$	0.31	0.51	27.	0.07	0.27	0.66

When including the new results for ^{56}Fe into the calculations for Table I, only minor changes from what was reported in Ref. [21] are observed. The GXPF1a interaction still performs better than the KB3G interaction, and rates based on the QRPA still deviate significantly from the rates based on the experimental strength distributions, especially at the lower density and temperature.

V. CONCLUSIONS

In summary, the GT transition strength distribution from ^{56}Fe to ^{56}Mn has been extracted using the ^{56}Fe$(t,^3$He$)$ reaction at 115 A MeV. The extraction was based on the empirical proportionality between the GT strengths and differential cross sections at zero momentum transfer for the $(t,^3$He$)$ probe. Since the resolution in excitation energy that was achieved was significantly better than that for existing (n,p) data from Ref. [26], transitions to 1^+ states at 0.11 and 1.17 MeV in ^{56}Mn could be separated and the corresponding GT strengths cleanly extracted.

The extracted GT strengths were compared with theory. Shell-model calculations with the GXPF1a and KB3G interactions reproduced the data well compared to calculations based on the QRPA. Since the theoretical strength distributions are used as inputs for calculating EC rates in astrophysical simulations of stellar environments, the derived EC rates were compared with EC rates derived from the experimental GT strength distributions. The new ^{56}Fe$(t,^3$He$)$ data are important for making reliable comparisons since the transition strengths to the states at 0.11 and 1.17 MeV are most important in the rate calculations. EC rate calculations based on GT strengths from the shell-model calculation with the GXPF1a interaction do better than those with the KB3G interaction in reproducing the EC rates based on the GT strengths extracted from the data. EC rates based on the GT strengths from the QRPA calculation are a poor match to the rates based on the experimental results.

These outcomes confirm previous results for nearby nuclei in the pf shell and add to the existing database for nuclei in this mass range for which detailed comparisons between theory and data are feasible, including derived electron-capture rates of relevance for astrophysical simulations.

ACKNOWLEDGMENTS

The authors would like to thank the staff at NSCL for their efforts and support of the experiment described in this manuscript. This work was supported by the US National Science Foundation [Grants No. PHY-1102511, No. PHY-0822648 (JINA), and No. PHY-1068217]. The work of Y.S. and M.N. was supported by the Uchida Energy Science Promotion Foundation.

[1] K. Langanke and G. Martínez-Pinedo, Rev. Mod. Phys. **75**, 819 (2003).
[2] H. A. Bethe, G. E. Brown, J. Applegate, and J. M. Lattimer, Nucl. Phys. A **324**, 487 (1979).
[3] A. Heger, K. Langanke, G. Martínez-Pinedo, and S. E. Woosley, Phys. Rev. Lett. **86**, 1678 (2001).
[4] W. R. Hix, O. E. B. Messer, A. Mezzacappa, M. Liebendörfer, J. Sampaio, K. Langanke, D. J. Dean, and G. Martínez-Pinedo, Phys. Rev. Lett. **91**, 201102 (2003).
[5] H.-T. Janka, K. Langanke, A. Marek, G. Martínez-Pinedo, and B. Müller, Phys. Rep. **442**, 38 (2007).
[6] K. Iwamoto, F. Brachwitz, K. Nomoto, N. Kishimoto, H. Umeda, W. R. Hix, and F.-K. Thielemann, Astrophys. J. Suppl. **125**, 439 (1999).
[7] F. Brachwitz *et al.*, Astrophys. J. **536**, 934 (2000).
[8] S. Gupta, E. F. Brown, H. Schatz, P. Möller, and K. Kratz, Astrophys. J. **662**, 1188 (2007).
[9] H. Schatz *et al.*, Nature (London) **505**, 62 (2013).
[10] G. M. Fuller, W. A. Fowler, and M. J. Newman, Astrophys. J. **42**, 447 (1980).
[11] G. M. Fuller, W. A. Fowler, and M. J. Newman, Astrophys. J. **252**, 715 (1982).
[12] G. M. Fuller, W. A. Fowler, and M. J. Newman, Astrophys. J. **48**, 279 (1982).
[13] G. M. Fuller, W. A. Fowler, and M. J. Newman, Astrophys. J. **293**, 1 (1985).
[14] P. Möller and J. Randrup, Nucl. Phys. A **514**, 1 (1990).
[15] J.-U. Nabi and H. V. Klapdor-Kleingrothaus, At. Data Nucl. Data Tables **88**, 237 (2004).
[16] N. Paar, G. Colò, E. Khan, and D. Vretenar, Phys. Rev. C **80**, 055801 (2009).
[17] A. A. Dzhioev, A. I. Vdovin, V. Y. Ponomarev, J. Wambach, K. Langanke, and G. Martínez-Pinedo, Phys. Rev. C **81**, 015804 (2010).
[18] Y. F. Niu, N. Paar, D. Vretenar, and J. Meng, Phys. Rev. C **83**, 045807 (2011).
[19] F. Osterfeld, Rev. Mod. Phys. **64**, 491 (1992).
[20] M. N. Harakeh and A. van der Woude, *Giant Resonances: Fundamental High-Frequency Modes of Nuclear Excitations* (Oxford University Press, New York, 2001).
[21] A. L. Cole, T. S. Anderson, R. G. T. Zegers, S. M. Austin, B. A. Brown, L. Valdez, S. Gupta, G. W. Hitt, and O. Fawwaz, Phys. Rev. C **86**, 015809 (2012).
[22] A. Poves, J. Sánchez-Solano, E. Caurier, and F. Nowacki, Nucl. Phys. A **694**, 157 (2001).
[23] M. Honma, T. Otsuka, B. A. Brown, and T. Mizusaki, Eur. Phys. J. A **25**, 499 (2005).
[24] M. Sasano *et al.*, Phys. Rev. Lett. **107**, 202501 (2011).
[25] M. Sasano *et al.*, Phys. Rev. C **86**, 034324 (2012).
[26] S. El-Kateb *et al.*, Phys. Rev. C **49**, 3128 (1994).
[27] T. Rönnqvist *et al.*, Nucl. Phys. A **563**, 225 (1993).
[28] F. Marti, P. Miller, D. Poe, M. Steiner, J. Stetson, and X. Y. Wu, AIP Conf. Proc. **600**, 64 (2001).
[29] D. J. Morrissey, B. M. Sherrill, M. Steiner, A. Stolz, and I. Wiedenhoever, Nucl. Instrum. Methods B **204**, 90 (2003).
[30] C. J. Guess *et al.*, Phys. Rev. C **83**, 064318 (2011).
[31] G. W. Hitt *et al.*, Nucl. Instrum. Methods A **566**, 264 (2006).
[32] D. Bazin, J. A. Caggiano, B. M. Sherrill, J. Yurkon, and A. Zeller, Nucl. Instrum. Methods B **204**, 629 (2003).

[33] H. Fujita *et al.*, Nucl. Instrum. Methods A **484**, 17 (2002).
[34] J. Yurkon, D. Bazin, W. Benenson, D. Morrissey, B. Sherrill, D. Swan, and R. Swanson, Nucl. Instrum. Methods A **422**, 291 (1999).
[35] G. W. Hitt *et al.*, Phys. Rev. C **80**, 014313 (2009).
[36] K. Makino and M. Berz, Nucl. Instrum. Methods A **427**, 338 (1999).
[37] G. Perdikakis *et al.*, Phys. Rev. C **83**, 054614 (2011).
[38] R. G. T. Zegers *et al.*, Phys. Rev. C **74**, 024309 (2006).
[39] A. L. Cole *et al.*, Phys. Rev. C **74**, 034333 (2006).
[40] R. G. T. Zegers *et al.*, Phys. Rev. Lett. **99**, 202501 (2007).
[41] R. G. T. Zegers *et al.*, Phys. Rev. C **77**, 024307 (2008).
[42] T. N. Taddeucci, C. A. Goulding, T. A. Carey, R. C. Byrd, C. D. Goodman, C. Gaarde, J. Larsen, D. Horen, J. Rapaport, and E. Sugarbaker, Nucl. Phys. A **469**, 125 (1987).
[43] H. Junde, H. Su, and Y. Dong, Nuclear Data Sheets **112**, 1513 (2011).
[44] J. Cook and J. Carr, Computer program FOLD, Florida State University (unpublished), based on F. Petrovich and D. Stanley, Nucl. Phys. A **275**, 487 (1977); modified as described in J. Cook, K. W. Kemper, P. V. Drumm, L. K. Fifield, M. A. C. Hotchkis, T. R. Ophel, and C. L. Woods, Phys Rev. C **30**, 1538 (1984); R. G. T. Zegers, S. Fracasso, and G. Coló (unpublished).
[45] M. A. Hofstee *et al.*, Nucl. Phys. A **588**, 729 (1995); S. Y. van der Werf, computer code NORMOD, KVI Groningen, 1991 (unpublished).
[46] B. A. Brown, W. D. M. Rae, E. McDonald, and M. Horoi, NUSHELLX@MSU, http://www.nscl.msu.edu/~brown/resources/resources.html; W. D. M. Rae, NUSHELLX, http://www.garsington.eclipse.co.uk/.
[47] B. A. Brown, Phys. Rev. C **58**, 220 (1998).
[48] S. C. Pieper and R. B. Wiringa, Annu. Rev. Nucl. Part. Sci. **51**, 53 (2001); R. B. Wiringa (private communication).
[49] W. G. Love and M. A. Franey, Phys. Rev. C **24**, 1073 (1981).
[50] M. A. Franey and W. G. Love, Phys. Rev. C **31**, 488 (1985).
[51] J. Kamiya *et al.*, Phys. Rev. C **67**, 064612 (2003).
[52] S. Y. van der Werf, S. Brandenburg, P. Grasdijk, W. A. Sterrenburg, M. N. Harakeh, M. B. Greenfield, B. A. Brown, and M. Fujiwara, Nucl. Phys. A **496**, 305 (1989).
[53] D. Frekers, Nucl. Phys. A **752**, 580 (2005).
[54] G. Martínez-Pinedo, A. Poves, E. Caurier, and A. P. Zuker, Phys. Rev. C **53**, R2602 (1996).
[55] P. Möller, J. Nix, W. Myers, and W. Swiatecki, At. Data Nucl. Data Tables **59**, 185 (1995).
[56] A. D. Becerril Reyes, S. Gupta, H. Schatz, K.-L. Kratz, and P. Möller, in *Proceedings on International Symposium on Nuclear Astrophysics-Nuclei in the Cosmos-IX, 2006*, edited by J. Cederkall *et al.*, PoS (NIC-IX) 075.
[57] A. Heger, K. Langanke, G. Martínez-Pinedo, and S. E. Woosley, Astrophys. J. **560**, 307 (2001).
[58] K. Langanke and G. Martínez-Pinedo, Nucl. Phys. A **731**, 365 (2004).